ELSEVIER

Materials Science and Engineering B 149 (2008) 152–158

MATERIALS SCIENCE & ENGINEERING B

www.elsevier.com/locate/mseb

Review

Studies on passive and active silver–sodium ion-exchanged glass waveguides and devices

S. Yliniemi [a], Q. Wang [b], J. Albert [c], S. Honkanen [a,b,*]

[a] *Micro and Nanosciences Laboratory, Helsinki University of Technology, Finland*
[b] *College of Optical Sciences, University of Arizona, USA*
[c] *Department of Electronics, Carleton University, Ottawa, Canada*

Received 23 October 2007; accepted 19 November 2007

Abstract

In this paper, we review our recent work on exploring and developing new techniques for planar lightwave circuits utilizing silver–sodium ion exchange. In the experiments, two special kinds of glass substrates have been used: aluminoborosilicate glass (also called BGG31) specially developed for passive ion-exchanged waveguides and phosphate glass (commercial name IOG-1) designed for waveguide laser applications. Phosphate glass can be doped with large amounts of rare earth ions without significant lifetime reduction. This enables fabrication of short-cavity waveguide lasers, a desirable feature for example in high-repetition rate modelocked lasers operating at 1550 nm wavelength region. Birefringence properties of buried molten salt ion-exchanged waveguides in BGG31 glass are presented in detail. Photosensitivity properties of both undoped and Er–Yb-codoped IOG-1 glass are discussed. A new approach to fabricate waveguide Bragg gratings through UV exposure in IOG-1 glass will be presented.

Keywords: Ion exchange; Glass waveguide; Photosensitivity; Waveguide laser

Contents

1. Introduction

Ion exchange in glass substrates is an old and well-known technique in optics. In ion-exchange process the alkali cations in glass (typically Na^+, K^+, and Ca^{2+}) are exchanged to other cations with the same valence (Ag^+, Rb^+, Cs^+, Li^+, K^+, and Tl^+). Being a diffusion-driven process, ion exchange produces a gradient like concentration profile. Also, due to the differing polarizabilities and sizes between the exchanged ions, it produces a refractive index change in glass. These phenomena can be utilized in fabrication of inexpensive graded index (GRIN) lenses widely applied in small photocopiers, scanners, endoscopes and in collimation optics in high power diode lasers, as well as in planar lightwave circuits used in telecommunication

* Corresponding author at: Micro and Nanosciences Laboratory, Helsinki University of Technology, 02015 Espoo, Finland. Tel.: +358 9 451 4193.
E-mail address: seppo.honkanen@tkk.fi (S. Honkanen).

0921-5107/$ – see front matter © 2008 Published by Elsevier B.V.
doi:10.1016/j.mseb.2007.11.032

backbone and metropolitan area networks. Ion exchange has also been used in glass coloring.

This paper concentrates on exploring silver–sodium ion-exchanged glass waveguides with a special emphasis in the study of birefringence in these waveguides and the utilization of ion-exchanged waveguide cavities in laser applications. Reducing or even eliminating the effect of birefringence in planar lightwave circuits is essential for minimizing the polarization dependent loss. Since standard singlemode fibers used in telecommunication networks are not polarization maintaining, also the connecting waveguide components need to show polarization independent operation. In this paper, we will show how the properties of ion-exchanged waveguides can be used to reduce waveguide birefringence significantly.

Telecommunication networks require cheap and compact transmitters in the 1550 nm wavelength region. Several these kinds of transmitters have been recently demonstrated in erbium–ytterbium doped phosphate glass substrates [1–3]. Phosphate glass is an ideal host for rare-earth ions because of its high solubility of rare-earth ions without significant lifetime reduction of the upper laser level. Most recent waveguide laser applications in phosphate glass utilize Bragg gratings fabricated by lithographic procedures or thin-film reflectors attached straight to the waveguide facets. Both of these cavity mirror solutions involve multiple steps in the clean room, and are therefore time-consuming and expensive approaches. In this paper we will show how this can be avoided by utilization of Bragg grating inscription into phosphate glass by UV irradiation through phase masks. UV-written Bragg gratings are nowadays widely deployed in fibers and fiber lasers but the use of UV-written Bragg gratings in integrated optical waveguide lasers has awaited, because it has turned out to be difficult to write gratings into glass material that provides enough gain in short cavity lengths (phosphate glass). Also, UV-written Bragg gratings improve the laser efficiency since UV-written volume Bragg gratings are nearly lossless and do not couple pump laser light out from surface waveguides. In this paper, we will review our results on photosensitivity in phosphate glass, and also present a waveguide laser in phosphate glass utilizing a UV-written Bragg grating as another cavity mirror.

2. Low birefringence waveguides in aluminoborosilicate glass

When an isotropic material (like glass) is subject to mechanical stress it may become optically anisotropic resulting in stress-induced birefringence. Stress can be either compressive or tensile. Typically compressive stress increases the refractive index while tensile stress has the opposite effect [4]. In ion-exchanged waveguides, stress is built in since the exchanged ions have different ionic radii and also because the thermal expansion of the exchanged glass region and the substrate glass are different [5]. In a channel waveguide the stress distribution built up during the waveguide fabrication is anisotropic and has dependence on both x- and y-coordinates:

$$\sigma_x(x, y) \neq \sigma_y(x, y) \neq \sigma_z(x, y),$$

where σ_x, σ_y and σ_z are the stress components along x-, y-, and z-axis (x-axis being normal to the surface). Since diffusion has greater ingress in the y-direction than in the x-direction, and because the waveguide can slightly expand along the normal to the surface, the stress component in the x-direction is smaller than in the y-direction ($\sigma_x < \sigma_y$) [5]. The refractive indices for quasi-TE- and quasi-TM-modes depend on the stress components σ_x, σ_y and σ_z in the following way [5]:

$$n_{\mathrm{TE}} = n_0 + C_1\sigma_y + C_2(\sigma_x + \sigma_z),$$
$$n_{\mathrm{TM}} = n_0 + C_1\sigma_x + C_2(\sigma_y + \sigma_z),$$

where n_0 refers to refractive index without stress, and C_1 and C_2 are the elasto-optical coefficients of the glass (note that $C_2 > C_1$ in most glasses [5–7], and here C_1 and C_2 are taken as positive, therefore for compressive stress $\sigma_y > 0$). It has been observed that in Ag^+–Na^+ ion-exchanged waveguides $n_{\mathrm{TM}} > n_{\mathrm{TE}}$, indicating compressive stress [5,8].

Along with stress-induced birefringence, the asymmetric refractive index profile of a typical ion-exchanged waveguide also contributes to the waveguide birefringence. This type of birefringence is called form birefringence. Form birefringence produces greater effective refractive index for the quasi-TE mode because the index profile has wider lateral dimensions. In diffused waveguides, form birefringence can be reduced by waveguide burial and/or by thermal annealing that shape the index profile to a more symmetric direction. Burial also reduces the effect of surface on form birefringence, resulting in a more symmetric index profile.

The waveguides were fabricated into BGG31 glass by molten salt ion exchange followed by a burial process [9,10]. Aluminoborosilicate glass BGG31 was specifically developed to fulfill the requirements of ion-exchanged waveguides in passive (i.e., undoped) glass [11]. Burial was performed for 2400 s at $T = 250\,^{\circ}\mathrm{C}$ with an applied field of 640 V/mm. Due to the differing self-diffusion coefficients, wider waveguides get buried deeper. With the burial parameters used in fabrication, the depth of the waveguides with mask opening widths from 2 to 10 μm varied from 5.6 to 6.8 μm. The waveguide birefringence was defined using a difference interferometer approach described in Ref. [12]. Results before annealing are presented in Fig. 1 (filled circles). It can be observed from Fig. 1 that birefringence for all waveguide widths is low, of the order of 10^{-5} or below. As expected, waveguide birefringence increases as a function of mask opening width, which is mainly due to increasing form birefringence. For all waveguide widths, the effective index of the quasi TE-mode is larger than the effective index of the quasi TM-mode, i.e., $n_{\mathrm{eff,TE}} > n_{\mathrm{eff,TM}}$.

The effect of annealing on waveguide birefringence is also shown in Fig. 1. Annealing, for 15 min at 250 °C, reduces the waveguide birefringence only slightly. However, the effect of 45 min total annealing is already significant. Birefringence is of the order of 10^{-6} or below, and interestingly, birefringence

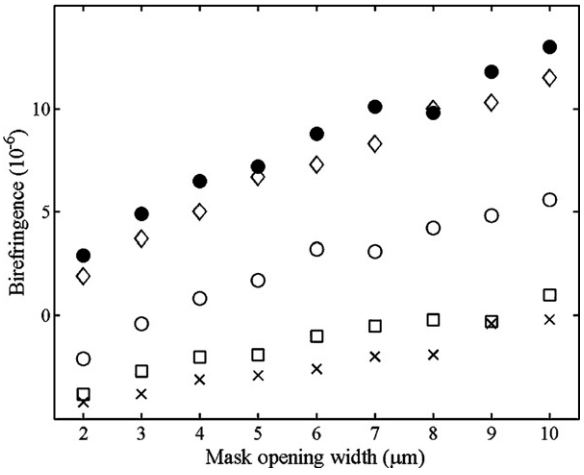

Fig. 1. Waveguide birefringence ($n_{\mathrm{eff,TE}} - n_{\mathrm{eff,TM}}$) for different mask opening widths. Filled circles refer to waveguides before annealing, diamonds to waveguides annealed for 15 min at 250 °C, open circles to waveguides annealed for 45 min, squares to waveguides annealed for 75 min, and crosses to waveguides annealed for 105 min.

for the two narrowest waveguides has changed the sign, meaning $n_{\mathrm{eff,TM}} > n_{\mathrm{eff,TE}}$. Annealing for another half an hour gives $n_{\mathrm{eff,TM}} > n_{\mathrm{eff,TE}}$ for all the mask opening widths. Further annealing starts to show signs of saturation, which was expected. As it was explained above, stress-induced birefringence favors higher effective index for TM-mode while form birefringence favors TE-mode. During annealing, ions forming a waveguide diffuse further, and the mode profile becomes more symmetric reducing form birefringence. With long enough annealing, the effect of form birefringence approaches its minimum and the residual birefringence is primarily due to stress-induced effects. Narrow waveguides show higher residual birefringence than the wider ones. This can be either due to the more pronounced stress-induced birefringence in narrow waveguides or due to higher form birefringence in wide waveguides. However, the birefringence dependence on waveguide width is less pronounced in case of residual birefringence.

2.1. Birefringence of the second order (odd) mode

Integrated optical add-drop multiplexers (OADMs) such as those suggested in Refs. [13–16] require low birefringence not only for the fundamental (even) but also for the second order (odd) mode. This is why it is important to define the second order mode birefringence, too. The difference interferometric approach utilized in measuring birefringence of the even mode could not be used in case of the odd mode because of the stability issues in coupling the odd mode into the waveguide, therefore, another measurement method was chosen. In this approach, a Bragg grating is utilized in order to measure the slightly different effective refractive indices of the quasi-TE and TM modes. According to the Bragg condition, reflection takes place at wavelengths given by

$$\lambda = 2n_{\mathrm{eff}}\Lambda,$$

where λ is the reflected wavelength, Λ is the period of the Bragg grating, and n_{eff} is the effective refractive index of the mode. Each mode has a characteristic effective refractive index, and therefore they are reflected at slightly different wavelengths. The modal birefringence therefore appears as a polarization dependent wavelength (PDW) shift given by

$$\Delta\lambda = 2\Lambda\,\Delta n_{\mathrm{eff}},$$

where $\Delta\lambda = \lambda_{\mathrm{TE}} - \lambda_{\mathrm{TM}}$ is the measured PDW shift and Δn_{eff} is the birefringence to be defined.

According to the manufacturer, the optical spectrum analyzer (OSA) (Ando, model AQ6317) used in these measurements has a resolution of 0.015 nm or better and a wavelength repeatability of 0.005 nm, which is equivalent to a minimum detectable PDW shift of 0.020 nm or better, corresponding to birefringence of 2×10^{-5}. The method described above also includes the possible effect of the grating induced birefringence. Bragg grating is a crucial part in most OADMs [14,15], and therefore it is important to study if the grating increases the polarization sensitivity of the device. Usually UV-exposure induces some birefringence on devices [17,18]. The results for even and odd mode birefringence as a function of mask opening width are shown in Fig. 2 [19]. It can be seen from the figure that birefringence

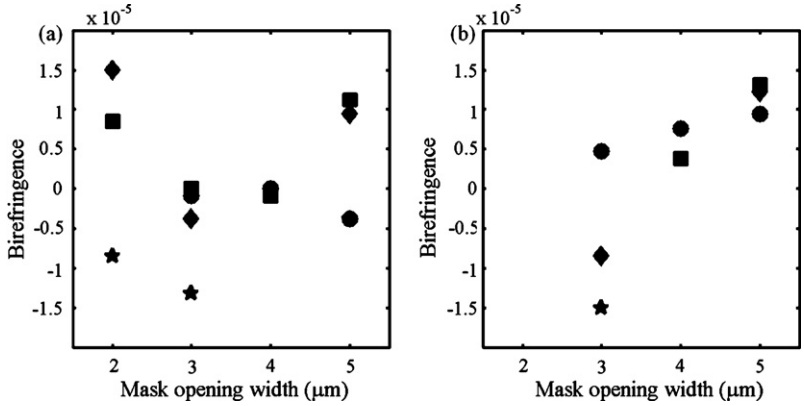

Fig. 2. Birefringence with a waveguide Bragg grating for different mask opening widths: (a) even and (b) odd mode. Squares, diamonds, circles and stars refer to different measurements from waveguides with the same mask opening width.

is below the measurement accuracy of the OSA, i.e., below 2×10^{-5}.

The above results suggest that buried Ag^+–Na^+ ion-exchanged waveguides have inherently low birefringence that can be further reduced by matching the form birefringence with the opposite sign stress induced birefringence through thermal annealing. It can be concluded that these ion-exchanged waveguides with birefringence of the order of 10^{-5} or below are suitable for most optical communications applications. It is noteworthy that low birefringence can be obtained for both the even (fundamental) and odd (second order) mode for a wide range of waveguide widths. This result has significance in integrated optical add-drop multiplexers, dispersion compensators, and all-optical packet header recognition chips. This low birefringence for both even and odd modes in a wide range of waveguide widths would be difficult to obtain with other media for integrated optics, such as silica-on-silicon, although birefringence issues have more or less been solved for single mode waveguides. Several approaches to reduce or compensate for birefringence have been suggested in connection with the leading waveguide technology, silica-on-silicon. Also, this low birefringence for both even and odd modes in a wide range of waveguide widths would be difficult to obtain in silica-on-silicon waveguides [20].

3. Photosensitivity in phosphate glass

Phosphate glass is favored in short fiber and waveguide amplifiers and lasers due to the high solubility of rare earth ions without a significant lifetime reduction of the upper amplifier/laser level. This enables high gain values in short cavity lengths and small mode volumes. However, it has turned out to be difficult to expose UV-written Bragg gratings in phosphate glass. First experiments reported by Pissadakis et al. [21] in ion-exchanged Er–Yb-codoped Schott IOG-1 glass demonstrated a thin surface grating operating in Raman–Nathan region with a refractive index change of 2×10^{-3}. Only a small index change of the order of 10^{-5} was observed in a pristine sample. This kind of a surface grating would not work as a mirror in waveguide lasers for two reasons: (1) surface grating at the pump input side would couple out the pump laser power at ~980 nm propagating close to the surface; (2) a surface grating with a relatively low index modulation would not provide enough optical feedback for lasing. In this paper, we review our recent experiments and developments in the studies of photosensitivity in phosphate glass [22,23]. Commercially available Schott IOG-1 phosphate glass was used in this work to study photosensitivity and to realize short cavity waveguide lasers.

3.1. Undoped (passive) IOG-1 glass

In Fig. 3, the transmission spectra from ultraviolet to near-infrared wavelengths are shown for undoped and Er–Yb codoped IOG-1 glass as well as for ion-exchanged undoped glass. Three things can be immediately observed from Fig. 3. First, almost no transmission is observed below wavelengths 230 nm for Er–Yb codoped and ion-exchanged glass, suggesting that absorption at

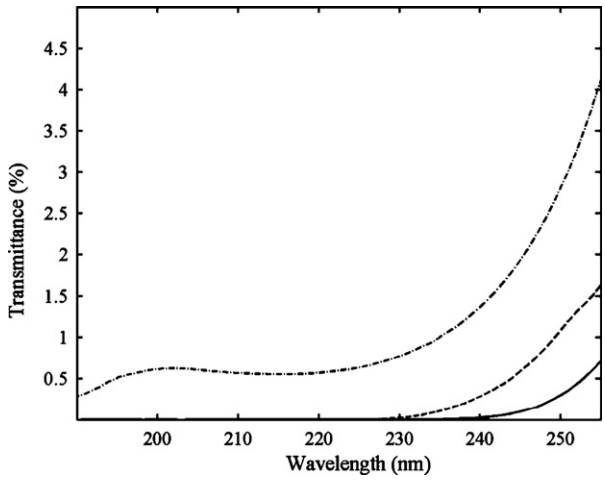

Fig. 3. UV–vis transmission spectra for passive IOG-1 (undoped, dash dotted line) and active IOG-1-7 (Er/Yb-codoped, dashed line), and for ion-exchanged passive IOG-1 (solid line) glass substrates. The thickness of the substrates was 1.5 mm.

those wavelengths is very high with all the irradiation below 230 nm being absorbed in a thin surface layer. Therefore, for the Er–Yr codoped glass the irradiation wavelength of 248 nm was chosen instead of 193 nm. For undoped glass, however, the irradiation wavelength of 193 nm is a better choice, as the transmission at the wavelength of 248 nm is already too high.

First experiments were carried out with undoped substrates in which waveguides were already fabricated. A phase mask with a period of 1015 nm and a length of 9 mm was used. The ArF excimer laser was run at 100 pps (pulses per second) with a fluence of ~460 mJ/cm^2. It was observed that a grating with reflectivity between 1 and 12% was obtained after a relatively short irradiation time of 4 min, with further irradiation erasing the grating. Clearly, these low grating reflectivities are not practical for mirrors in lasers applications. Stronger free-space diffraction efficiencies (measured by illuminating the sample by a He–Ne laser at different angles) were always measured at the sides of the waveguides where Ag^+ concentration is lower suggesting that Ag^+ and Ag^0 species might prevent irradiation from penetrating deep enough into the glass. In view of this, the grating irradiation was carried out with a pristine sample and the waveguides were fabricated only after writing of the grating. The laser was run in ArF mode with a fluence of 300 mJ/cm^2. Reflectance and transmittance spectra of the grating are shown in Fig. 4. Reflectance of 44% (calculated from the transmission dip) was reached with only a 4 mm long grating and 5 min exposure time. The measured reflectivity corresponds to an index modulation of 1.0×10^{-4} if a full overlap between the waveguide and grating fringes is assumed. The phase mask period was 1065 nm giving a reflectance peak at 1608 nm in undoped IOG-1 glass. The inspection of the grating before waveguide fabrication revealed that the grating is a volume grating operating in Bragg regime. The reflectance spectrum shows no coupling to the cladding modes. The small sidelobe observed on the long wavelength side of the main Bragg peak in Fig. 4 results from a slight nonuniformity in the UV-writing beam along the length of the grating and from the fact that the gratings were not apodized.

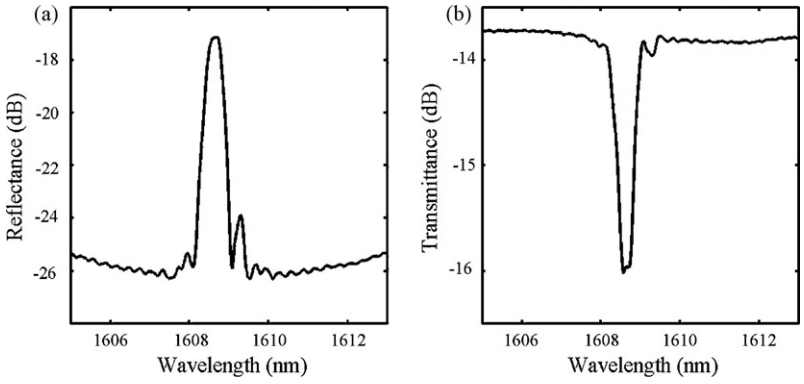

Fig. 4. (a) Reflectance and (b) transmittance spectra for a waveguide grating in undoped IOG-1 glass. Grating reflectivity is equal to 44%. This value was calculated from the transmission dip.

For the application considered here (narrowband reflector for waveguide laser), the presence of such sidelobes has no effect whatsoever on device performance as long as the resulting net gain at the sidelobe wavelength does not allow lasing action. The fact that we do not have to apodize the gratings simplifies their fabrication considerably.

These experiments show that it is possible to write high quality Bragg gratings into passive IOG-1 glass, and reflectances high enough for waveguide laser applications can be achieved simply by increasing the grating length.

3.2. Er–Yb-codoped (active) IOG-1 glass

The waveguides in active IOG-1 glass were fabricated only after the grating exposure. UV writing was performed with a fluence of 250 mJ/cm^2 for 30 min at a wavelength of 248 nm. The highest grating reflectance produced in this way was only 15% with a grating length of 13 mm corresponding to an index modulation of 1.5×10^{-5}. The polarization dependent wavelength shift of the grating was equal to 0.02 nm corresponding to birefringence of the order of 10^{-4}, as expected for a surface waveguide. The grating operates in Bragg regime, but the index modulation is too low for laser quality gratings. The significantly lower index modulation compared with the one obtained with an ArF laser emitting at 193 nm into undoped glass is most probably due to the combined effect of the poorer coherence properties of the excimer laser system at 248 nm along with the fact that absorption at 248 nm is weaker in Er–Yb codoped glass compared with absorption in undoped glass at 193 nm.

3.3. Waveguide DBR laser with UV-written Bragg grating

Fabrication of a high quality volume grating in Er–Yb-codoped phosphate glass is indeed a complex task. With improved optical coherence, volume waveguide gratings with maximum reflectance of only 15% were obtained. For typical laser applications, however, reflectance above 70% should be obtained, which is why another approach was adopted. As we have seen in above, it is possible to write narrow-band high reflectance waveguide gratings into undoped IOG-1 glass. In view of this, we made use of hybrid glass which is a substrate composed of both Er–Yb-codoped and undoped parts bonded to each other [24]. The Bragg grating was written to the undoped part of the hybrid substrate, and it served as a wavelength selective cavity mirror, as well as, the output coupler of the laser. The Er–Yb-codoped part of the hybrid glass provided the gain required for the laser operation. The Er- and Yb-concentrations were 1.0×10^{20} and 6.0×10^{20} ions/cm^3, respectively. The Bragg grating was written through a phase mask with an ArF pulsed excimer laser. Unlike in the case of the fabrication of the grating with reflectivity of 44% (Fig. 4), beam expanders were used. This resulted in improved spatial coherence but reduced the fluence to 140 mJ/cm^2. The exposure time was 30 min and the laser was run at a frequency of 100 pps. A phase mask with a period of 1065 nm was designed so that the Bragg grating in IOG-1 glass would have a peak reflectance at ~1535 nm corresponding to the gain maximum of Er-doped glass. The waveguide was fabricated after the grating writing.

In Fig. 5, the transmission spectra of a 1-cm long waveguide grating for both quasi TE- and TM-polarizations are presented. The transmission minimum occurs at 1534.71 nm (TE) and at

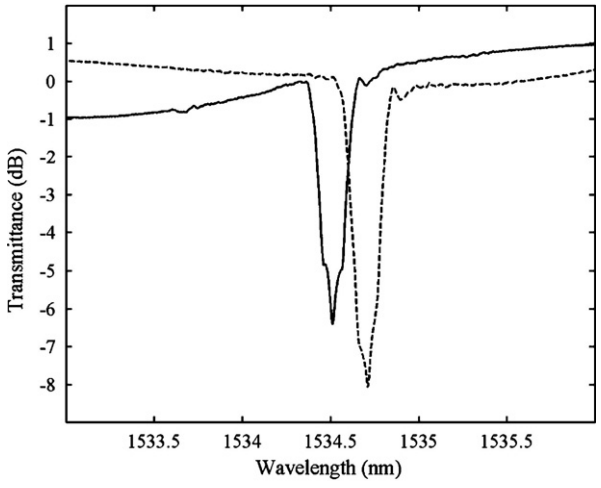

Fig. 5. Transmission spectra of a UV-written waveguide Bragg grating. The dashed line refers to quasi TE-polarization and the solid line refers to quasi TM-polarization.

1534.52 nm (TM) with a peak reflectance of 80%. The grating period (533 nm) calculated from the Bragg law corresponds well with the phase mask period divided by two (the theoretical period produced into glass). A polarization dependent wavelength shift of 0.2 nm was observed corresponding to a waveguide birefringence of $\sim 10^{-4}$. This is not surprising for a surface waveguide in which the proximity of the surface causes more form birefringence than in buried waveguides where birefringence is of the order of 10^{-5} or below.

In laser experiments, a fiber coated with a SiO_2/TiO_2-thin film stack aligned with the waveguide facet in the Er–Yb-codoped part of the substrate was used as the other cavity mirror. Pump power from a fiber-pigtailed semiconductor diode laser emitting at 980 nm was also delivered through this fiber. The thin film stack was designed to have transmittance close to 100% at the pump wavelength of 980 nm and reflectance close to 100% at 1550 nm wavelength region.

Since the post-bake annealing could reduce significantly the strength of the UV-written grating, the annealing was performed at 225 °C in three steps. After each annealing step, the laser performance was tested. Also the Er–Yb-codoped waveguide length was shortened between the annealing steps. It was deduced from the green light emission (due to ESA) that all available pump power was consumed in a length shorter than the waveguide length in the Er–Yb-codoped part of the substrate, the rest of the Er–Yb-codoped part of the waveguide being underpumped and adding therefore to losses. Shortening the sample increased pump efficiency resulting in improved output power and reduced threshold power. As expected, the threshold power required for lasing steadily decreased with sample annealing and shortening, while the output power and the slope efficiency increased. During annealing, the silver ions diffuse further into glass. Annealing also increases the mode size and smoothens the index profile, therefore reducing coupling and propagation losses. In addition, it improves the mode overlap between the pump and the signal. After the first annealing step, lasing was obtained only when using two pump lasers (the output signal was separated from the pump signal using a 980/1550 WDM-coupler). After the final annealing step, an output power of 9.0 mW could be extracted from the sample with a pump power of 200 mW the threshold being 135 mW. Slope efficiency was 13.9%. The laser output power as a function of pump power is presented in Fig. 6. Annealing altogether for 120 min at 225 °C did not reduce the grating strength. The lasing wavelength decreased from 1534.77 to 1534.50 nm with annealing because the effective index of the propagating mode decreases due to smaller maximum refractive index difference, a characteristic feature of diffused waveguides. In the inset of Fig. 6, the laser output spectrum revealing a singlemode operation is presented. The OSA resolution was 0.07 nm. Output power of 9 mW is high enough to provide good SNR but still low enough to avoid undesirable nonlinear effects in optical fibers.

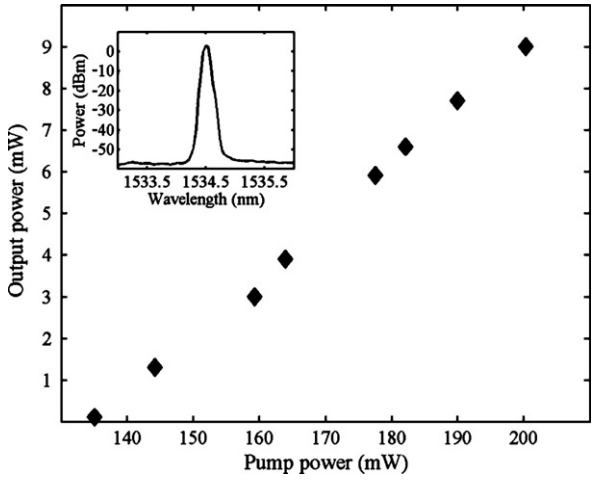

Fig. 6. DBR laser output power of as a function of pump power. DBR laser utilizes a waveguide Bragg grating as a wavelength selective element as well as another mirror. The laser output spectrum is presented in the inset.

4. Summary and outlook

A method for fabricating waveguides with negligible birefringence has been demonstrated. This method includes waveguide burial and thermal postbake annealing. Low waveguide birefringence has been demonstrated for both fundamental (even) and second order (odd) mode for a wide range of waveguide widths. This approach can be utilized to fabricate waveguide components (such as OADMs) with polarization independent operation.

An extensive study on photosensitivity properties of phosphate glass has been carried out. High quality narrowband waveguide gratings in undoped phosphate glass have been demonstrated. A singlemode waveguide laser utilizing a UV-written grating as another mirror was demonstrated in hybrid phosphate glass. The waveguide Bragg grating was written with a pulsed ArF excimer laser emitting at 193 nm. A waveguide grating in Er–Yb-codoped phosphate glass with a reflectivity of 15% has been demonstrated, this time written with a KrF excimer laser emitting at 248 nm. In both cases, the Bragg grating was exposed prior to waveguide fabrication process. It was assumed that silver particles produced during ion exchange prevents UV light from penetrating deep enough into the glass to form a volume grating. This conclusion is supported by the UV–vis transmission measurements carried out with both pristine and ion-exchanged phosphate glass substrates. However, a thin surface grating with reflectivity of about 12% could be produced in an existing ion-exchanged waveguide. Future work includes developing stronger Bragg gratings in Er–Yb-codoped phosphate glass as this would enable fabrication of compact, narrow linewidth distributed feedback lasers at multiple wavelengths on a single chip.

Acknowledgements

The authors wish to thank David Geraghty, Jose Castro, Michael Morrell and Albane Laronche for their contributions to the experiments and fruitful discussions. Funding from the Academy of Finland, the State of Arizona Photonics Initiative (TRIF), the Magnus Ehrnrooth Foundation and the Canada Research Chairs program is also acknowledged.

References

[1] S. Blaize, L. Bastard, C. Cassagnètes, J.E. Broquin, IEEE Photon. Technol. Lett. 15 (2003) 516–518.
[2] P. Madasamy, G. Nunzi Conti, P. Pöyhönen, M.M. Morrell, D.F. Geraghty, S. Honkanen, N. Peyghambarian, Opt. Eng. 41 (2002) 1084–1086.
[3] D.L. Veasey, D.S. Funk, P.M. Peters, N.A. Sanford, G.E. Obarski, N. Fontaine, M. Young, A.P. Peskin, W.-C. Liuand, S.N. Houde-Walter, J.S. Hayden, J. Non-Cryst. Solids 263/264 (2000) 369–381.
[4] J. Albert, G.L. Yip, Electron. Lett. 23 (1987) 737–738.
[5] A. Brandenburg, J. Lightwave Technol. 4 (1986) 1580–1593.
[6] D. Heiman, D.S. Hamilton, R.W. Hellwarth, Phys. Rev. B 19 (1979) 6583–6592.
[7] A.N. Miliou, R. Srivastava, R.V. Ramaswamy, Appl. Opt. 30 (1991) 674–681.
[8] J.T.A. Carriere, J.A. Frantz, B.R. Youmans, S. Honkanen, R.K. Kostuk, IEEE Photon. Technol. Lett. 16 (2004) 1134–1136.
[9] S. Yliniemi, B.R. West, S. Honkanen, Appl. Opt. 44 (2005) 3358–3363.
[10] P. Madasamy, B.R. West, M.M. Morrell, D.F. Geraghty, S. Honkanen, N. Peyghambarian, Opt. Lett. 28 (2003) 1132–1134.
[11] L. Ross, Glastech. Ber. 62 (1989) 285–297.
[12] W. Lukosz, C. Stamm, Sens. Actuators A 25 (1991) 185–188.
[13] A. Tervonen, S. Honkanen, S.I. Najafi, Opt. Eng. 32 (1993) 2083–2091.
[14] D.F. Geraghty, D. Provenzano, M. Morrell, S. Honkanen, A. Yariv, N. Peyghambarian, Electron. Lett. 37 (2001) 829–831.
[15] J.M. Castro, D.F. Geraghty, B.R. West, S. Honkanen, Appl. Opt. 43 (2004) 6166–6173.
[16] J.M. Castro, D.F. Geraghty, B.R. West, S. Honkanen, C.M. Greiner, D. Iazikov, T. Mossberg, Appl. Opt. 45 (2006) 1236–1243.
[17] T. Erdogan, V. Mizrahi, J. Opt. Soc. Am. B 11 (1994) 2100–2105.
[18] H.G. Limberger, P.-Y. Fonjallaz, R.P. Salathé, Appl. Phys. Lett. 68 (1996) 3069–3071.
[19] S. Yliniemi, J. Albert, A. Laronche, J.M. Castro, D. Geraghty, S. Honkanen, Appl. Opt. 45 (2006) 6602–6606.
[20] K. Wörhoff, C.G.H. Roeloffzen, R.M. de Ridder, G. Segno, L.T.H. Hilderink, A. Driessen, Proc. SPIE 5451 (2004) 369–380.
[21] S. Pissadakis, A. Ikiades, P. Hua, A.K. Sheridan, J. Wilkinson, Opt. Exp. 12 (2004) 3131–3136.
[22] S. Yliniemi, S. Honkanen, A. Ianoul, A. Laronche, J. Albert, J. Opt. Soc. Am. B 23 (2006) 2470–2478.
[23] S. Yliniemi, J. Albert, Q. Wang, S. Honkanen, Opt. Exp. 14 (2006) 2898–2903.
[24] S.D. Gonzone, J.S. Hayden, D.S. Funk, A. Roshko, D.L. Veasey, Opt. Lett. 26 (2001) 509–511.